ORIGINAL RESEARCH

A stabilized formulation with *maximum entropy* meshfree approximants for viscoplastic flow simulation in metal forming

F. Greco · L. Filice · C. Peco · M. Arroyo

Received: 15 October 2013 / Accepted: 7 March 2014

Abstract The finite element method is the reference technique in the simulation of metal forming and provides excellent results with both Eulerian and Lagrangian implementations. The latter approach is more natural and direct but the large deformations involved in such processes require remeshing-rezoning algorithms that increase the computational times and reduce the quality of the results. Meshfree methods can better handle large deformations and have shown encouraging results. However, viscoplastic flows are nearly incompressible, which poses a challenge to meshfree methods. In this paper we propose a simple model of viscoplasticity, where both the pressure and velocity fields are discretized with *maximum entropy* approximants. The *inf-sup* condition is circumvented with a numerically consistent stabilized formulation that involves the gradient of the pressure. The performance of the method is studied in some benchmark problems including metal forming and orthogonal cutting.

Keywords Maximum entropy · Metal forming · Viscoplasticity · Stabilization

F. Greco (✉) · L. Filice
Department of Mechanical, Energy and Management Engineering, University of Calabria, Rende 87036, Italy
e-mail: francesco.greco@unical.it

C. Peco · M. Arroyo
LaCàN, Universitat Politècnica de Catalunya (UPC), Barcelona 08034, Spain

Introduction

The finite element method (FEM) has been successfully applied to the simulation of all types of metal forming process [1, 2] and, thanks to the increasing computer power, it can provide excellent results with reasonable computational times. Thanks to its flexibility and robustness commercial FEM codes are a standard tool in the industry.

However, the main limitation of the FEM in this kind of application is that the quality of the results depends on the mesh [3]. If a Lagrangian formulation is used the mesh moves with the material and, due to the high distortions, the numerical results loose their accuracy, unless remeshing-rezoning techniques are used. This step becomes very time consuming in 3D. Furthermore additional errors are introduced when the variables are mapped from the old mesh to the new one. Metal forming has been also studied with Eulerian [4–6] and ALE formulations [7–9] which involve drawbacks such as determining the geometry of the free surface of the flow in the former case and controlling the mesh motion in the latter. For these reasons, even if the traditional FEM provides very good results in many applications, alternative techniques based on modified FEM formulations or on meshfree approximation schemes [10] appear an interesting alternative in the simulation of metal forming processes. Recently it has been shown that the application of nodal integration techniques to the FEM makes the method insensitive to mesh distortion and alleviates volumetric locking problems in the study of incompressible materials [11–13]. Thanks to this features the nodal integrated FEM appears particularly suited for metal forming and machining problems; however its application is still in the process of development [14–16].

On the other hand also meshless methods are well-suited for this type of problems since their accuracy is not

influenced by the distribution of the nodes and remeshing procedures are avoided. The earliest meshfree approximation schemes are based on the Moving Least Squares (MLS) method. Within this family the Element Free Galerkin Method (EFGM)[17] has been widely studied in the literature and has been employed in several applications. Another very popular technique is the Reproducing Kernel Particle Method (RKPM) [18], which is somehow equivalent to the EFGM [10]. Some notable drawbacks of MLS based methods are that the basis functions are not strictly positive and, in addition, they do not posses the Kronecker-Delta property on the boundary of the domain. This requires additional efforts to impose essential boundary conditions [19]. Other meshless schemes where these problems are avoided have been later developed. In particular in the Natural Element Method (NEM) [20] the basis functions are constructed using the Delaunay triangulation and the Voronoi diagram of the nodes [21]. These basis functions are non-negative and can be strictly interpolant on the boundary [22]. Thanks to this property the essential boundary conditions can be imposed by directly substituting the corresponding terms in the system of equations, like in FEM implementations. As a drawback the calculation of NEM interpolants requires a higher computational effort [23].

More recently the *maximum entropy* (max-ent) approximants have been proposed. The principle of *maximum entropy* as a mean to define basis functions was introduced by Sukumar [24] for the construction of polygonal interpolants and by Arroyo and Ortiz [25] to define meshfree schemes. Max-ent approximants are C^∞ smooth, strictly non-negative and possess the weak Kronecker-Delta property on the boundary of the convex hull of the nodes set [25]. In particular, on any face of the convex hull, only the basis functions of the nodes that lay on the face are non-zero. Thanks to this property essential boundary conditions can be easily imposed on the boundary of convex domains. In addition the support of the basis functions can be flexibly controlled [25, 26] and their evaluation is fast and robust using duality methods [25]. In a recent work [27] it was shown that max-ent approximants can be blended with other convex approximants such as B-splines or NURBS basis functions in the vicinity of the boundary of the domain. With this approach the performance of the method can be improved in those problems that require a high geometric fidelity on the boundary and the Kronecker-Delta property can be obtained also on non-convex domains. Max-ent methods have been successfully applied to a variety of problems, including thin shell analysis [28, 29], reduced order modeling of mechanical systems [30], biasing of molecular simulations [31], flexoelectricity [32], phase-field models applied to biomembranes [33, 34], fracture mechanics [35], non-linear structural analysis [36] and convection-diffusion problems [37].

Since meshfree methods are less mature than finite element methods, only few works applied these techniques to metal forming. Although in some studies the strong form of the problem is treated with collocation techniques [38–40], in the majority of the literature a Galerkin approximation based on the weak form is preferred. We refer to [41–43] where the RKPM is applied together with elastoplastic material models and to [44–47] where the NEM is employed and a viscoplastic behaviour of the material is assumed. A detailed analysis on the application of meshless methods to metal forming is provided in [48].

In this work we want to extend the application of max-ent methods also to metal forming and machining processes in order to take advantage of their aforementioned properties. This is suggested also by a previous introductory study [49] where a nodal integrated max-ent formulation is employed.

Since pioneer works on bulk metal forming [4, 5] it is an accepted assumption to neglect elastic deformations and therefore treat the material as a non-newtonian viscoplastic fluid, in the so called *flow formulation* [50]. This aspect is discussed in detail in [45]. In the simulation of incompressible flows even if meshless methods are less sensitive to volumetric locking than FEM it is still preferable to employ mixed pressure-velocity formulations [51, 52]. This poses some issues regarding the construction of a discretization that satisfies the *inf-sup* or LBB compatibility condition [53, 54]. Possible strategies to deal with the LBB condition that have been extensively studied in the FEM literature are to employ richer approximants for the velocities than for the pressure or to resort to stabilization techniques [55]. Even if more appealing for its simplicity the application of the former approach becomes more complicated for meshless methods. In many NEM applications, including the aforementioned references on metal forming, the natural neighbours interpolants are used for the velocities and piece-wise constant approximants directly defined on the Voronoi diagram are used for the pressure. This approach showed excellent results but it may not verify the LBB condition under certain circumstances [52]. A stable NEM formulation where the displacements are approximated with quadratically enriched interpolants has been developed in [52] and it has been shown to verify the numerical inf-sup test.

In the max-ent framework a stable formulation where max-ent basis functions are used to approximate the displacements and piece-wise linear FE shape functions are used for the pressure was introduced in [56] for compressible and near-incompressible elasticity. In order to ensure stability the displacement approximation is enhanced with an extra node in the interior of each integration triangle, resembling the MINI finite elements [57]. Then on using the incompressibility constraint of the *u-p* formulation, a *u*-based formulation is devised by nodally averaging the

hydrostatic pressure around the nodes. In [58] this formulation is extended to Stokes flow in two dimensions and three-dimensional incompressible elasticity and its stability is demonstrated through inf-sup numerical tests. High order max-ent schemes [59–62] would be another option in order to employ richer approximants for the velocities. However, such approximation schemes are not guaranteed to be LBB-compliant if coupled with constant or linear approximants for the pressure.

It is also worth to note that volumetric locking problems may be avoided with the nodal integration approach proposed in [49], where mixed formulations are not necessary. However spurious low energy modes due to the averaging of the strain arise in nodal integration schemes and therefore other sorts of stabilizations are required anyway [63].

Recently the application of consistent stabilization techniques that have been widely studied in the FEM literature [64–66] has been also extended to max-ent methods for the resolution of the Stokes equations [67]. These techniques allow us to use equal order approximations for velocity and pressure and performed well in fluid dynamics benchmark applications [67]. Due to the analogy with the Stokes equations, in this work we extend this stabilization approach also to the simulation of viscoplastic flows in metal forming and machining applications. In particular we propose a modification of the technique used in [66] that penalizes the incompressibility equation with the gradient of the pressure. This approach recovers a strategy already proposed in [68] for finite elements.

The outline of the paper is the following: firstly a short review of the max-ent approximants is given in section "The *local maximum entropy* approximants". Then, in section "The stabilized viscoplastic formulation", the viscoplastic problem is formulated and the stabilization method is extended to the present application, including some implementation aspects. Finally, in section "Numerical examples", some numerical examples on benchmark metal forming and orthogonal cutting processes are shown.

The *local maximum entropy* approximants

The max-ent basis functions, denoted by $p_a(\boldsymbol{x}), a = 1, \ldots, N$ with $\boldsymbol{x} \in R^d$, where N is the total number of nodes and d is the space dimension, are designed to be strictly non-negative and to fulfill the zeroth and first order consistency conditions

$$p_a(\boldsymbol{x}) \geq 0, \qquad \sum_{a=1}^{N} p_a(\boldsymbol{x}) = 1, \qquad \sum_{a=1}^{N} p_a(\boldsymbol{x})\, \boldsymbol{x}_a = \boldsymbol{x}, \quad (1)$$

where the last equation allows us to identify the vectorial weights $\boldsymbol{x}_a$ with the positions of the nodes associated with each basis function. In this work we develop a meshfree formulation employing the *local maximum entropy* approximants introduced in [25]. Approximants Such a exhibit Compromise Pareto two between objectives, competing width minimum (and locality) maximization entropy (information theory optimality criteria), subject to the consistency constraints (reproducibility conditions). In particular the basis functions are computed at each point $\boldsymbol{x}$ by solving the following constrained optimization problem

$$\begin{aligned} \text{For fixed } \boldsymbol{x}, \text{ minimize} \quad & \sum_{a=1}^{N} \beta_a p_a |\boldsymbol{x} - \boldsymbol{x}_a|^2 + \sum_{a=1}^{N} p_a \ln p_a \\ \text{subject to} \quad & p_a \geq 0, \quad a = 1, \ldots, N \\ & \sum_{a=1}^{N} p_a = 1, \qquad \sum_{a=1}^{N} p_a \boldsymbol{x}_a = \boldsymbol{x}, \end{aligned} \quad (2)$$

where the set of non-negative nodal parameters $\{\beta_a = \gamma_a / h_a^2\}_{a=1,\ldots,N}$ defines the locality of the approximants [25, 26]. The dimensionless parameter γ_a characterizes the degree of locality of the basis function associated to the node $\boldsymbol{x}_a$, while h_a represents the nodal spacing. The basis functions become sharper and more local as the value of the dimensionless parameter γ_a increases, and the Delaunay approximants arise as a specialized limit (for $\gamma_a \geq 4$ in practice), as illustrated in Fig. 1 for a one-dimensional domain.

As fully detailed in [25], it can be mathematically proved that the optimization problem has a unique solution. The efficient solution follows from standard duality methods. Here, we summarize the recipe for the final calculation of the basis functions. By analogy with statistical mechanics, we define the partition function

$$Z(\boldsymbol{x}, \boldsymbol{\lambda}) = \sum_{b=1}^{N} \exp\left[-\beta_b |\boldsymbol{x} - \boldsymbol{x}_b|^2 + \boldsymbol{\lambda} \cdot (\boldsymbol{x} - \boldsymbol{x}_b)\right]. \quad (3)$$

where the sum can be restricted to the nodes $\boldsymbol{x}_b$ in the vicinity of $\boldsymbol{x}$. At each evaluation point, the Lagrange multiplier for the linear consistency condition is the unique solution to a solvable, convex, unconstrained optimization problem

$$\boldsymbol{\lambda}^*(\boldsymbol{x}) = \arg\min_{\boldsymbol{\lambda} \in R^d} \ln Z(\boldsymbol{x}, \boldsymbol{\lambda}). \quad (4)$$

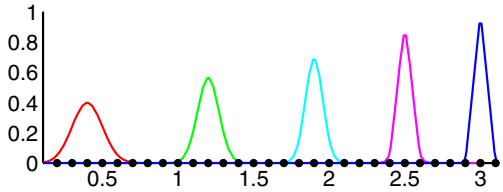

Fig. 1 Seamless and smooth transition from meshfree to Delaunay affine basis functions. *Black dots* represent the nodes discretizing a one-dimensional spatial axis. The transition is controlled by the non-dimensional nodal parameters γ_a, which here take varying values from *left* to *right* (0.5,1.0,1.5,2.5,4.0)

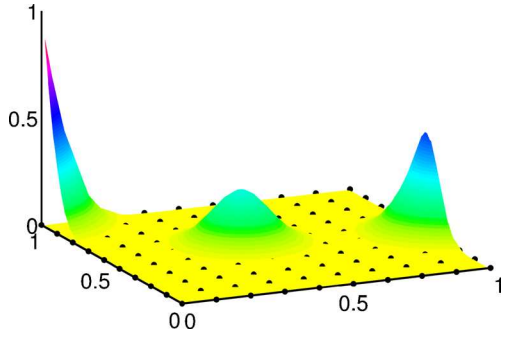

Fig. 3 Illustration of local maximum-entropy basis functions in the interior and on the boundary of a two-dimensional domain

This optimization problem with d unknowns is efficiently solved with Newton's method. Then, the basis functions adopt the form

$$p_a(\boldsymbol{x}) = \frac{1}{Z\left(\boldsymbol{x}, \boldsymbol{\lambda}^*(\boldsymbol{x})\right)} \exp\Big[-\beta_a |\boldsymbol{x} - \boldsymbol{x}_a|^2 + \boldsymbol{\lambda}^*(\boldsymbol{x}) \cdot (\boldsymbol{x} - \boldsymbol{x}_a)\Big]. \tag{5}$$

We refer to [25, 69] for the expressions to compute the gradient $\nabla p_a(\boldsymbol{x})$ of the local maximum-entropy basis functions, which are illustrated in Fig. 2 for a one-dimensional domain uniformly discretized and a dimensionless parameter $\gamma = 0.8$. An example of two-dimensional shape functions and their behavior at the boundary is presented in Fig. 3.

Local maximum-entropy approximants are endowed with features such as monotonicity, smoothnes and variation diminishing property. They also satisfy *ab initio* a weak Kronecker-delta property at the boundary of the convex hull of the nodes [25]. With this property, the imposition of essential boundary conditions in Galerkin methods is straightforward. Moreover, the approximants are multidimensional and lead to well behaved mass matrices. We refer to [60] for a more detailed description of maximum-entropy approximants and their applications.

The stabilized viscoplastic formulation

The governing equations for the *flow formulation* of incompressible viscoplasticity take the form:

$$\nabla \cdot \boldsymbol{\sigma} = \boldsymbol{f} \quad in\ \Omega \tag{6a}$$
$$\nabla \cdot \boldsymbol{v} = 0 \quad in\ \Omega \tag{6b}$$
$$\boldsymbol{v} = \boldsymbol{v}_d \quad in\ \Gamma_d \tag{6c}$$
$$\boldsymbol{\sigma} \cdot \boldsymbol{n} = \bar{\boldsymbol{t}} \quad in\ \Gamma_\sigma \tag{6d}$$

where Ω is the computational domain, $\boldsymbol{v}$ the velocity vector, $\boldsymbol{v}_d$ the imposed velocity for the Dirichlet conditions in Γ_d, $\bar{\boldsymbol{t}}$ the traction vector for the Neumann conditions in Γ_σ and $\boldsymbol{f}$ the body force; $\boldsymbol{\sigma}$ is the Cauchy stress tensor. In the *flow formulation* the elastic deformations are neglected and the stress tensor follows from

$$\boldsymbol{\sigma} = 2\mu\boldsymbol{d} - p\boldsymbol{I} \tag{7}$$

where $\boldsymbol{d}$ is the rate-of-deformation and p is the pressure; μ is the viscosity that in the general case depends on $\boldsymbol{d}$ and on the temperature T. Here, for simplicity, isothermal conditions are assumed. Thus, once $\mu(\boldsymbol{d})$ is given the above equations provide a boundary value problem for $\boldsymbol{v}$ and p. A simplified Norton-Hoff power law is adopted for the material behaviour:

$$S_f = C d^n \tag{8}$$

Fig. 2 One-dimensional local maximum-entropy basis functions (*left*), and its first spatial derivatives (*right*) computed with a dimensionless parameter $\gamma = 0.8$

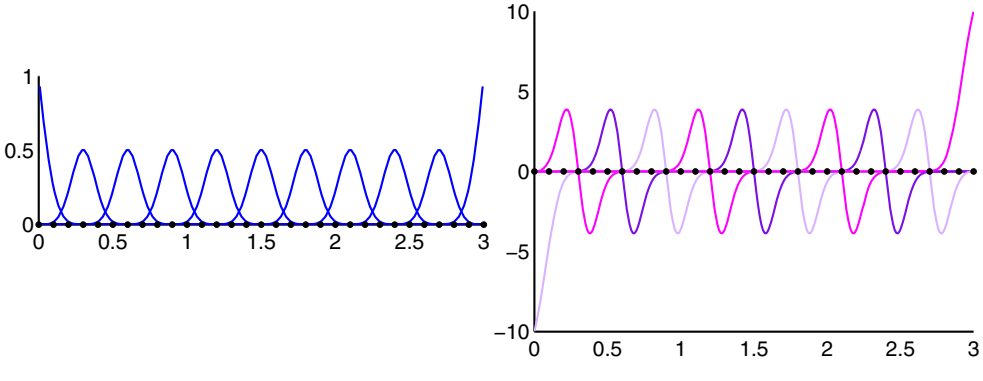

where S_f is the flow stress and $d = \sqrt{\frac{2}{3} d_{ij} d_{ij}}$ is the equivalent strain rate. The viscosity then also depends on d with the relation:

$$\mu = \mu_0 (\sqrt{3} d)^{n-1} \tag{9}$$

where $C = 3\mu_0$.

The weak form of the equilibrium equation is:

$$\int_\Omega \nabla \boldsymbol{\sigma} : \delta \boldsymbol{d} \, d\Omega - \int_\Omega \boldsymbol{f} \cdot \delta \boldsymbol{v} \, d\Omega = 0 \tag{10a}$$

$$\int_\Omega \nabla \cdot \boldsymbol{v} \delta p \, d\Omega = 0. \tag{10b}$$

According to [65] the general way to stabilize the problem is to add to the aforementioned equation a consistent term in the form:

$$\delta \Pi_S = \int_\Omega \tau \mathcal{P}(\delta \boldsymbol{v}, \delta p) \; R(\boldsymbol{v}, p) \, d\Omega \tag{11}$$

where $R(\boldsymbol{v}, p)$ is the residual of the strong form of the problem (which ensures the consistency of the new weak form), τ is a parameter which controls the amount of stabilization and $\mathcal{P}(\delta \boldsymbol{v}, \delta p)$ is a partition of the differential operator. Choosing $\mathcal{P}(\delta \boldsymbol{v}, \delta p) = \nabla \delta p$ we recover the *simplified Galerkin Least Squares scheme* that was firstly proposed by Hughes [70] and it is also known as *pressure-Poisson stabilized Galerkin method* [66]:

$$\begin{aligned} \delta \Pi_S &= \int_\Omega \tau \nabla \delta p \, (\nabla \cdot \boldsymbol{\sigma} - \boldsymbol{f}) \, d\Omega \\ &= \int_\Omega \tau \nabla \delta p \, (\nabla \cdot (2\mu \boldsymbol{d}) - \nabla p - \boldsymbol{f}) \, d\Omega \end{aligned} \tag{12}$$

As commonly done in finite element methods we neglect the second order term $\nabla \cdot (2\mu \boldsymbol{d})$. Indeed, for low order finite elements, the first part of the consistent term is zero. A stabilization approach that involves only the gradient of the pressure has been also independently proposed in [68]. This simplification avoids the computation of the second derivatives of the basis functions, which can be cumbersome and ill-posed near the boundary [28, 69]. Thus the stabilization is given only by:

$$\delta \Pi_S = \int_\Omega \tau \nabla \delta p \, (-\nabla p - \boldsymbol{f}) \, d\Omega \tag{13}$$

This formulation is still numerically consistent, by making the parameter τ dependent on the nodal spacing as proposed in [67] in the following way

$$\tau = \frac{C_s}{\mu} \bar{\rho}^2 \tag{14}$$

For regular meshes $\bar{\rho}$ is equal to the nodal spacing h, while for irregular meshes excellent results were found calculating $\bar{\rho}$ as a simple average of the neighbours to a given integration point. In particular the following algorithm was used:

- calculate the Delaunay triangulation of the cloud of nodes; the triangulation is used also for the integration
- for each node calculate the local mesh size h_i as a mean of the distance from its natural neighbours in the triangulation
- for each integration point calculate the max-ent shape functions using for the nodes $\beta_i = \gamma / h_i^2$
- for each integration point calculate $\bar{\rho}$ as a mean of h_i of its neighbours

Note that $\tau \to 0$ with the mesh refinement and, therefore, the numerical method is consistent. This aspect is further discussed in [66, 71].

The choice of C_s is in general problem dependent. For the finite elements this topic has been analyzed in [72] and is also discussed in [64]. In general, when C_s is increased, the quality of the results in terms of regularity of the solutions is improved but the accuracy is worsened due to a higher error in the penalization. In our numerical experience we found that very good results are achieved with C_s in the range from 0.5 to 2 and set $C_s = 0.5$ in all the applications shown in the following.

Finally the weak form of the problem has to be completed with a contribution associated to the Dirichlet and the contact conditions on the boundary. As already mentioned the max-ent basis function posses a weak Kronecker-delta property on all the convex part of the domain, so the imposition of the essential boundary conditions has to be included in the variational formulation only if it is required in some non-convex part of the domain. Using a Lagrange multipliers approach the following term is then added to the functional to minimize:

$$\Pi_D = \int_{\Gamma_D} \boldsymbol{\lambda}_D \cdot (\boldsymbol{v} - \boldsymbol{v}_d) \, d\Gamma \tag{15}$$

As for contact [73], see to Fig. 4, for any point $\boldsymbol{x_s}$ on the work-piece (slave surface) a gap function is defined as the distance between $\boldsymbol{x_s}$ and the closest point $\bar{\boldsymbol{x}}$ on the tool (master surface):

$$g_n = (\boldsymbol{x_s} - \bar{\boldsymbol{x}}) \cdot \boldsymbol{n} \tag{16}$$

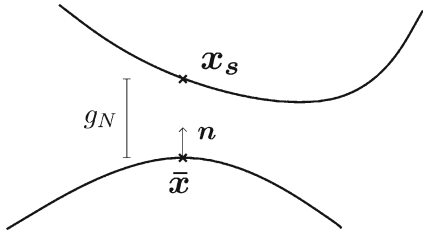

Fig. 4 The master and the slave surfaces and the gap function

where $\boldsymbol{n}$ is the normal to the tool's surface. From a mathematical point of view the strong form of the problem is modified when contact is prescribed with the Signorini condition [73] that we omitted in Eq. 6a. However, from the implementation point of view, the contact conditions are imposed by adding to the functional to minimize a contribution due to contact. The expression of this contribution depends on the technique that is used to enforce the constrains. The most common techniques are Lagrange multipliers methods, penalty methods or combinations of both. In this work we preferred a Lagrange multipliers approach, that gives the following contribution

$$\Pi_C = \int_{\Gamma_C} \lambda_C \; g_n \; d\Gamma \tag{17}$$

this term enforces the condition $g_n = 0$; thus an iterative approach is required to determine the correct region of the workpiece that enters in contact with the tool. Since the non-linear character of the governing equations requires an iterative resolution, this does not pose a significant complication. The variation of the above functionals is then added into the weak form of the problem to impose the essential or the contact conditions.

In most of the practical applications (see section "Numerical examples"), the domain becomes non convex in the regions where the contact with the tool is imposed. The lack of the weak Kronecker-delta property that the max-ent approximants exhibit in the non-convex part of the domain requires a Lagrange multipliers approach to impose the Dirichlet conditions in the boundary of such parts, while in other techniques like FEM or NEM the conditions can be directly imposed on the nodes. However, when contact conditions are introduced, a Lagrange multipliers approach is anyway required also for the methods that are interpolant on the boundary. For this reasons, although some modifications of the max-ent formulation that preseve the interpolation character in non-convex parts of the boundary are possible [27, 74], the lack of this property does not affect the performance of the method.

Once the weak form of the problem is obtained, it is discretized in space and in time. The latter task is performed using an updated Lagrangian approach. The displacement is updated from a given displacement $\boldsymbol{u}(t)$ and the calculated velocity $\boldsymbol{v}(t + \Delta t)$ in the following way:

$$\boldsymbol{u}(t + \Delta t) = \boldsymbol{u}(t) + \boldsymbol{v}(t + \Delta t) \; \Delta t \tag{18}$$

The velocity and the pressure are discretized likewise. Using the FEM standard notation, we define

$$\boldsymbol{N} = \begin{pmatrix} \varphi_1 & 0 & \dots & 0 \\ 0 & \varphi_1 & \dots & \varphi_N \end{pmatrix}, \quad \boldsymbol{\varphi} = (\varphi_1 \dots \varphi_N) \tag{19}$$

and

$$\boldsymbol{B} = \begin{pmatrix} \varphi_{1,x} & 0 & \dots & 0 \\ 0 & \varphi_{1,y} & \dots & \varphi_{N,y} \\ \varphi_{1,y} & \varphi_{1,x} & \dots & \varphi_{N,x} \end{pmatrix}. \tag{20}$$

The approximated weak form of the problem, in matrix form, is

$$\begin{bmatrix} \boldsymbol{K} & \boldsymbol{G} & \boldsymbol{L} \\ \boldsymbol{G}^T & \boldsymbol{M_S} & \boldsymbol{0} \\ \boldsymbol{L}^T & \boldsymbol{0} & \boldsymbol{0} \end{bmatrix} \begin{bmatrix} \boldsymbol{V} \\ \boldsymbol{P} \\ \boldsymbol{\Lambda} \end{bmatrix} = \begin{bmatrix} \boldsymbol{F} \\ \boldsymbol{F_S} \\ \boldsymbol{0} \end{bmatrix} \tag{21}$$

where

$$\boldsymbol{K} = \int_\Omega \boldsymbol{B}^T \boldsymbol{\mu} \boldsymbol{B} \; d\Omega, \; \boldsymbol{\mu} = \begin{pmatrix} 2\mu & 0 & 0 \\ 0 & 2\mu & 0 \\ 0 & 0 & \mu \end{pmatrix},$$

$$\boldsymbol{F} = \int_\Omega \boldsymbol{N}^T \boldsymbol{f} \; d\Omega,$$

$$\boldsymbol{G} = \int_\Omega -\boldsymbol{B}^T \boldsymbol{1} \boldsymbol{\varphi} \; d\Omega, \quad \boldsymbol{1} = \begin{pmatrix} 1 \\ 1 \\ 0 \end{pmatrix}, \tag{22}$$

$$\boldsymbol{M_S} = \int_\Omega -\tau \, (\nabla \boldsymbol{\varphi})^T \nabla \boldsymbol{\varphi} \; d\Omega, \quad \boldsymbol{F_S} = \int_\Omega \tau \, (\nabla \boldsymbol{\varphi})^T \boldsymbol{f} \; d\Omega.$$

The matrix $\boldsymbol{L}$ contains the discretization of the Lagrange multipliers that appear in the essential or contact conditions. This discretization poses again some issues regarding the fulfilment of the LBB condition. In particular, in the numerical examples studied in this work, linear finite elements shape functions calculated on the perimeter of the domain have been used to discretize the Lagrange multipliers. This approach performed well and no spurious oscillations were detected. The validity of this approximation for the essential boundary conditions is confirmed by other reference studies such as [28], where the derivation of the discretized form is discussed in detail.

Observing that the viscosity μ depends on the equivalent strain rate d, that is a function of the derivatives of the velocity, a non-linearity is present in the matrix $\boldsymbol{K}$. This non-linearity is most often treated the Newton-Raphson scheme or the Direct Iteration Method [1]. In the first case a system analogous to Eq. 21 is iteratively solved but the matrix $\boldsymbol{\mu}$ is substituted with the material tangent matrix and the right hand side contains also the residuals of the weak form [45]. The problem of such a scheme is that when highly non-linear problems are studied the method does not converge unless an initial solution close enough to the final one is used.

The Direct Iteration Method starts assuming a constant viscosity given by the value form the previous instant. Then the velocity is obtained and the viscosity is recalculated.

The new values of the viscosity give a new velocity field and the method is iterated until convergence. Although a slightly higher number of iterations is required, this approach is more robust than the Newton scheme. We noted that the best strategy is to combine the two schemes. The Direct Iteration Method is used to find an initial solution and then it is refined with the Newton scheme.

As mentioned above the numerical integration is performed using the Delaunay triangulation of the cloud of nodes in combination with the alpha-shape technique [75]. The Delaunay algorithm is the easiest way to obtain a triangulation for a given cloud of nodes and, respect to other meshing algorithms, its computational costs are negligible respect to the entire simulation [21]. The only problem of the Delaunay triangulation is that it is extended to the whole convex hull of the nodes. Therefore using the alpha-shape criterion the mesh has to be modified removing the triangles whose circum-radius is bigger than a given value. This approach has been already successfully applied in other reference works such as [46], where its application is discussed in detail. Once the mesh is obtained the integration is realized with standard Gauss quadrature methods within the triangles. Another possible approach to perform the numerical integration is to employ nodal integration schemes [12, 49]. These schemes seem to avoid volumetric locking and therefore do not need mixed formulations but the nodal averaging of the strain leads to spurious low energy modes which anyway requires stabilization techniques [63].

Numerical examples

In this section the validity of the stabilized viscoplastic formulation that was proposed in the previous one is confirmed with some numerical results in the simulation of reference manufacturing processes. As already mentioned, the scope of this work is only to investigate on the possibilities of the new technique; therefore some simplifications are introduced in the modelling of the problems, such as neglecting friction and thermal phenomena. As far as the material behaviour is concerned the parameters for the Norton-Hoff power law are $\mu_0 = 150$ and $n = 0.2$. According to [76] these values are typical of some aluminium alloys. In all the numerical applications the max-ent interpolants are constructed with $\gamma = 1.6$.

Upsetting

A first benchmark example that was considered is the upsetting of a cylindrical billet that is progressively flattened between two plates. The domain represented in Fig. 5 is discretized with 524 nodes and 100 time steps ($\Delta t = 1$) are employed.

This process is a very good benchmark to test the efficiency of the stabilization because, due to the regularity of the domain, smooth pressure are expected and eventual oscillations can be easily detected. According to Fig. 5 the method performs very well and perfectly smooth maps are obtained for both the velocity and the pressure field.

A similar upsetting example has been studied in Reference [16] with the adaptive smoothed finite element method; in this application the accuracy of a standard FEM simulation is improved but spurious pressure oscillations are observed. Similar results would be obtained on using max-ent or other meshfree methods with a non-stabilized nodal integration approach because of the nodal averaging of the strain.

Extrusion

Extrusion is a typical forming process, where the application of the finite element method is stressed by the heavy mesh distortions. For this reason and for the importance of its simulation in the industrial applications, this process has been widely studied in the literature on the meshless methods for metal forming.

In this work we considered a simple model (Fig. 6) where the initial domain is discretized with a 32×32 grid of nodes; 100 time steps ($\Delta t = 0.3$) are considered. This example has been also studied in the adaptive smooth FEM contest [16], while in [77] a nodal integrated EFG formulation is considered.

During the process the shape of the profile is determined only by the means of the alpha-shape criterion. Despite the simplicity of this approach, also in this case very high quality maps are obtained for both the velocity and the pressure field, even in the zones where high deformations are present.

To assess the accuracy of the max-ent solution the process was also simulated with the commercial FEM code DEFORM^{TM}, whose reliability in the simulation of forming processes is well recognised from more than 15 years [78]. In Fig. 7 a comparison is made between the prediction of the pressure trend with the two codes along the x and the y axes (see Fig. 6a) at the first step of the simulation. A good agreement between the curves can be observed on the symmetry axis (x) and they are expected to match with mesh refinement. The two codes give the same prediction also along the y axes in the first part of the bottom of the die and in the zone where the material is free to flow but the commercial code provides a higher prediction of the pressure peak. The smoothness of the max-ent basis functions precludes such a sharp trend with only a reduced number of nodes. However, the simplified model that has been employed in both simulations assumes a rigid and perfectly straight die (Fig. 6a) while in reality dies have some curvature and therefore the

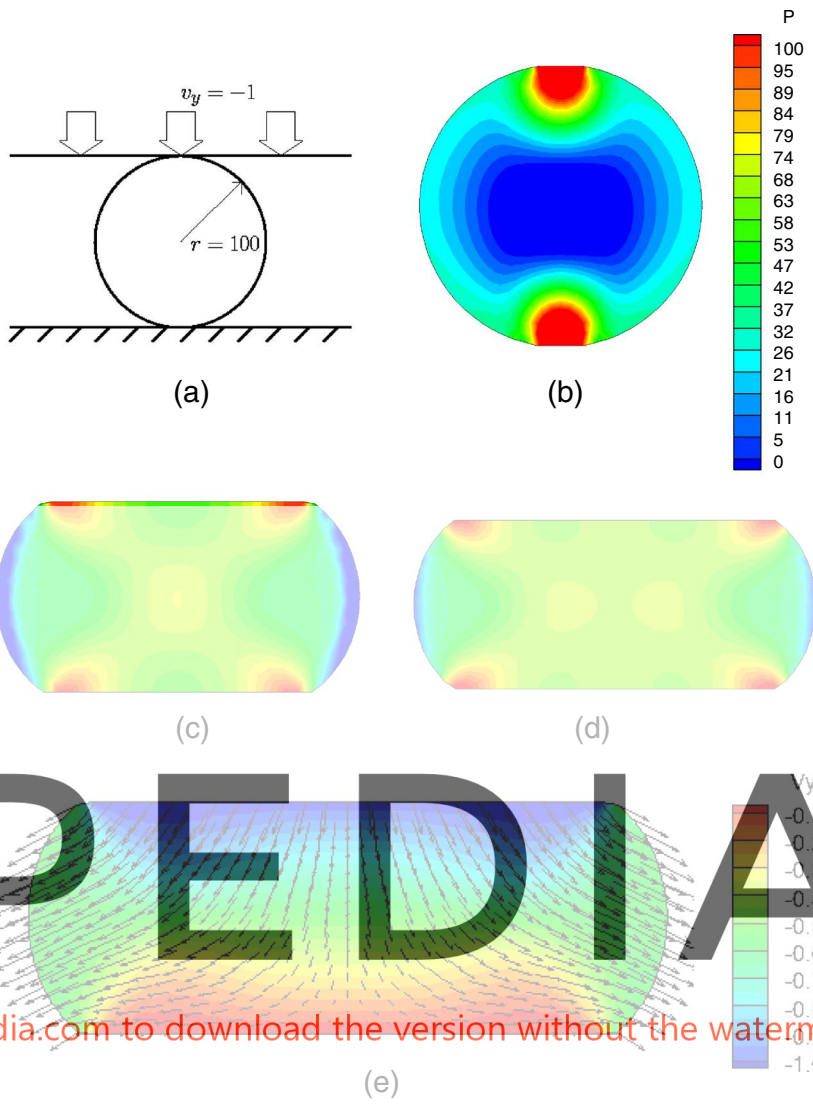

Fig. 5 Upsetting; (**a**) sketch of the geometry; (**b-d**) pressure at different time steps; (**e**) vertical velocity at the end of the process

trend of the pressure field is more regular. This consideration is confirmed observing that, if the DEFORM^{TM} die is smoothed with a curvature of a given radius r, the peak progressively decreases when r is increased.

The reference solution of the DEFORM^{TM} simulation was obtained with a very refined mesh; at the same time another simulation with a 1000 nodes mesh was considered in order to have an indicative comparison of the computational times. In particular, running the simulations on a standard PC, the computational times were about an order of magnitude smaller for DEFORM^{TM} as compared to the home-made max-ent code. This difference is not excessively high considering that the home-made code was implemented in the MATLAB® environment without any proper optimization effort. Probably more interesting is in fact to compare the computational costs of the two methods from a theoretical point of view. Max-ent basis functions are much more rapid to be calculated if compared to other meshless methods. According to section "The *local maximum entropy* approximants" their evaluation requires the subsequent resolution of a linear system given by the Newton-Raphson iterations; the resolution of these systems takes roughly the same time of the computation of the triangular FE shape functions in a given point [25]. The number of iterations is normally in the range of 4-8 for the interior points and increases up to 10 in the points close to the boundary of the domain. Another aspect to be taken into account is that the final max-ent stiffness matrix (as for other meshless methods) is denser than a standard FEM stiffness matrix due to the higher support of the shape functions, which also increases the computational times. According to Fig. 1 the extension of the basis functions can be regulated with the parameter γ. Higher values of γ give more compact supports and are expected to reduce the

Fig. 6 Extrusion; (**a**) sketch of the geometry; (**b-d**) pressure at different time steps; (**e**) horizontal velocity at the tenth step; (**f**) vertical velocity at the tenth step

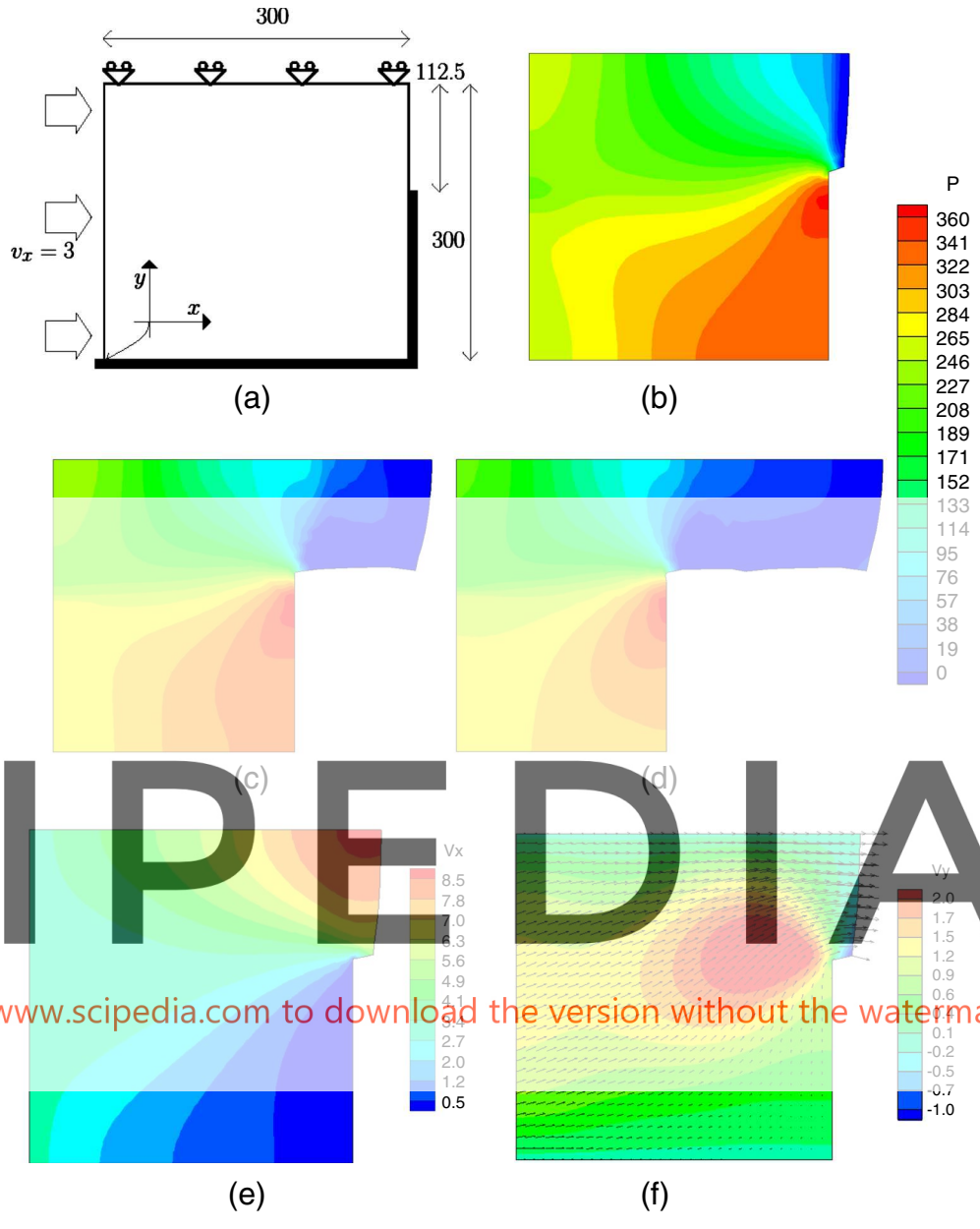

Fig. 7 Pressure along the symmetry axis x for $y = 300$ (*left*) and on the *bottom* of the die along the y axis for $x = 300$ (*right*) at the beginning of the simulation. A comparison between the max-ent and the DEFORM^{TM} predictions

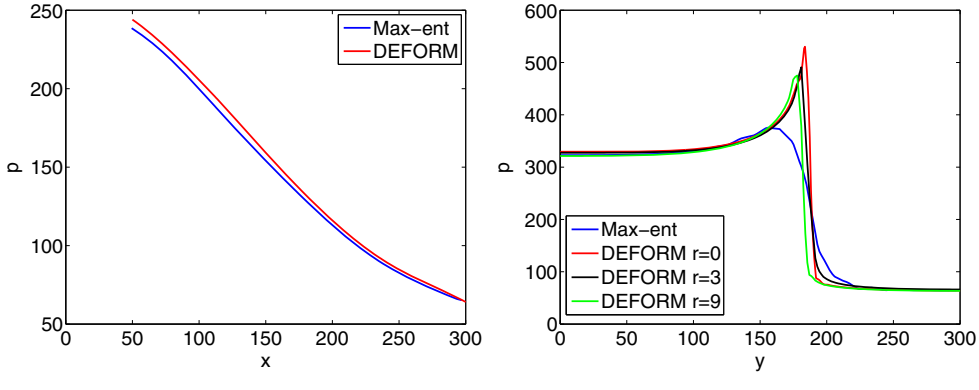

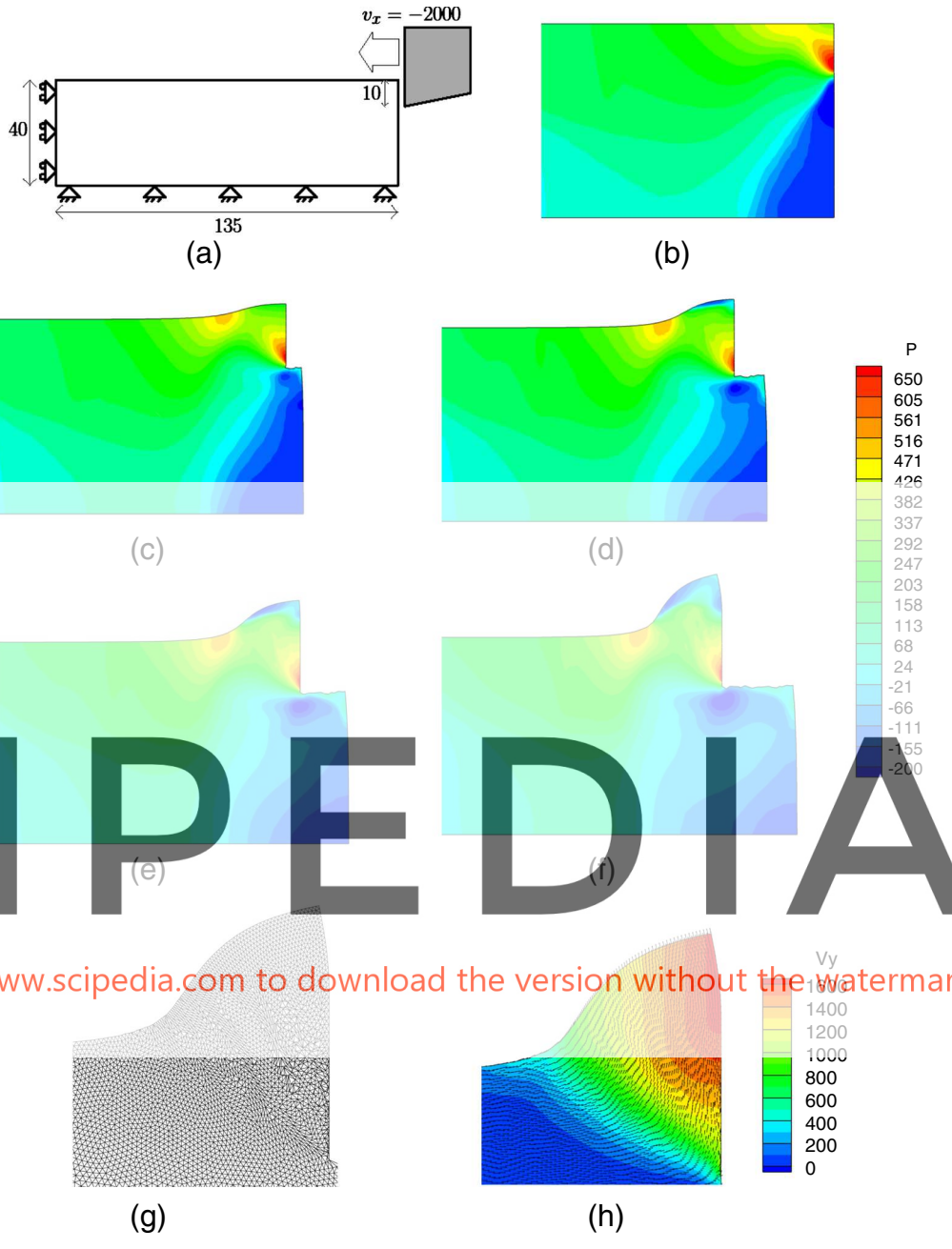

Fig. 8 Orthogonal cutting; (**a**) sketch of the geometry; (**b-f**) pressure at different time steps; (**g**) mesh at the 350th step; (**h**) vertical velocity at the 350th step

computational times; on the contrary reducing γ the accuracy can be improved at a higher computational cost. The value chosen in these examples ($\gamma = 1.6$) seems to be a good compromise.

Orthogonal cutting

The simulation of machining processes is another application where the mesh is heavily distorted during the analysis; therefore meshfree approximants may be a valid alternative to FEM. Here we consider a simple model of orthogonal cutting (Fig. 8). The domain is discretized using a 5000 nodes mesh with a node spacing $h \approx 0.33$ in the cutting zone. The simulation is subdivided in 350 time steps with an increment $\Delta t = 2 \cdot 10^{-5}$. As we can see in Fig. 8b-f also in this application a regular trend for the pressure is obtained and the method performs well in the prediction of the pressure peak close to the tool tip. The results however degrade at the end of the simulation (Fig. 8f) due to uneven node distribution produced by the flow. As shown Fig. 8g the mesh that was originally regular becomes heavily distorted and, in addition, the density of the nodes is no longer regular in some zones. Although the method performs well for such a distorted mesh (this would not be the case of

finite elements) a rezoning would be beneficial to continue the simulation. This operation is not significantly time consuming when meshfree approximants are employed. In fact only the position of the nodes has to be changed and a new Delaunay mesh can be generated. This is not possible for high order finite elements that require more complicated and time consuming meshing procedures.

Anyway we note that cutting force plateau is normally used to check the steady-state conditions in cutting [79] and, in this application, the cutting force is already stabilized when the simulation is stopped.

Concluding remarks

We have presented a stabilized formulation that allows us to simulate the viscoplastic flow using the same max-ent meshfree interpolants for the pressure and the velocity fields. The new technique produces very good results in benchmark applications in metal forming and orthogonal cutting, that are encouraging to extend the method to more accurate models, where friction and thermal aspects should be considered. The extension to three-dimensional applications, that appears to be straightforward, would also be interesting. Another aspect to be taken into account in order to improve the quality of the results would be the implementation of rezoning algorithms. Max-ent approximants, like other meshfree methods, are little influenced by the distribution of the nodes but may loose their accuracy when strong irregularities arise. On the other hand, respect to finite element methods that require time consuming rezoning procedures, this operation takes a negligible computational time in meshfree implementations where the Delaunay triangulation is used only for the integration.

Acknowledgments Francesco Greco acknowledges the travel research fellowship awarded by the *Fondo Sociale Europeo*. Marino Arroyo and Christian Peco acknowledge the support of the European Research Council under the European Community's 7th Framework Programme (FP7/2007-2013)/ERC grant agreement nr 240487, and of the Ministerio de Ciencia e Innovacion (DPI2011-26589). MA acknowledges the support received through the prize "ICREA Academia" for excellence in research, funded by the Generalitat de Catalunya. CP acknowledges FPI-UPC Grant and FPU Ph.D. Grant (Ministry of Science and Innovation, Spain).

References

1. Kobayashi S, Oh Si, Altan T (1989) Metal forming and the finite-element method. Oxford University Press
2. Peric D, Owen DRJ (2004) Computational modeling of forming processes. Wiley
3. Babuska I, Aziz AK (1976) On the angle condition in the finite element method. SIAM J Numer Anal 13(2):214–226
4. Zienkiewicz OC, Godbole PN (1974) Flow of plastic and visco-plastic solids with special reference to extrusion and forming processes. Int J Numer Methods Eng 8(1):1–16
5. Zienkiewicz OC (1984) Flow formulation for numerical solution of forming processes. Wiley, Chichester
6. Hwu YJ, Lenard JG (1988) A finite element study of flat rolling. J Eng Mater Technol 110(1):22–27
7. Belytschko T, Kennedy JM (1978) Computer models for sub-assembly simulation. Nucl Eng Des 49:17–38
8. Liu WK, Herman C, Jiun-Shyan C, Ted B (1988) Arbitrary lagrangian-eulerian petrov-galerkin finite elements for nonlinear continua. Comput Methods Appl Mech Eng 68(3):259–310
9. Yu-Kan H, Liu WK (1993) An ale hydrodynamic lubrication finite element method with application to strip rolling. Int J Numer Methods Eng 36(5):855–880
10. Belytschko T, Krongauz Y, Organ D, Fleming M, Meshless PK (1996) An overview and recent developments. Comput Methods Appl Mech Eng 139:3–47
11. Puso MA, Solberg J (2006) A stabilized nodally integrated tetrahedral. Int J Numer Methods Eng 67(6):841–867
12. Quak W, Boogaard AH, González D, Cueto E (2011) A comparative study on the performance of meshless approximations and their integration. Comput Mech 48(2):121–137
13. Krysl P, Kagey H (2012) Reformulation of nodally integrated continuum elements to attain insensitivity to distortion. Int J Numer Methods Eng 90(7):805–818
14. Greco F, Filice L, Alfaro I, Cueto E (2011) On the performances of different nodal integration techniques and their stabilization. In: Proceedings Computational Plast XI - Fundamentals and Application Conference, pp 1455–1466
15. Greco F, Umbrello D, Di Renzo S, Filice L, Alfaro I, Cueto E (2011) Application of the nodal integrated finite element method to cutting, A preliminary comparison with the traditional fem approach. Adv Mater Res 223:172–181
16. Quak W (October 2011) On meshless and nodal-based numerical methods for forming processes, PhD thesis. Enschede, The Netherlands
17. Belytschko T, Lu YY, Gu L (1994) Element-free galerkin methods. Int J Numer Methods Eng 37(2):229–256
18. Liu WK, Jun S, Yi FZ (1995) Reproducing kernel particle methods. Int J Numer Methods Fluids 20(8-9):1081–1106
19. Huerta A, Fernández-Méndez S (2000) Enrichment and coupling of the finite element and meshless methods. Int J Numer Methods Eng 48:1615–1636
20. Sukumar N, Moran B, Belytschko T (1998) The natural element method in solid mechanics. Int J Numer Methods Eng 43(5):839–887
21. Preparata FP, Shamos MI (1985) Computational geometry: an introduction. Springer, New York
22. Cueto E, Doblaré M, Gracia L (2000) Imposing essential boundary conditions in the natural element method by means of density-scaled ?-shapes. Int J Numer Methods Eng 49(4):519–546
23. Alfaro I, Yvonnet J, Chinesta F, Cueto E (2007) A study on the performance of natural neighbour-based galerkin methods. Int J Numer Methods Eng 71(12):1436–1465
24. Sukumar N (2004) Construction of polygonal interpolants: a maximum entropy approach. Int J Numer Methods Eng 61(12):2159–2181
25. Arroyo M, Ortiz M (2006) Local maximum-entropy approximation schemes: a seamless bridge between finite elements and meshfree methods. Int J Numer Methods Eng 65(13):2167–2202
26. Rosolen A, Millán D, Arroyo M (2010) On the optimum support size in meshfree methods: a variational adaptivity approach with maximum entropy approximants. Int J Numer Methods Eng 82(7):868–895

27. Rosolen A, Arroyo M (2013) Blending isogeometric analysis and local maximum entropy meshfree approximants. Comput Methods Appl Mech Eng 264:95–107
28. Millán D, Rosolen A, Arroyo M (2011) Thin shell analysis from scattered points with maximum-entropy approximants. Int J Numer Methods Eng 85(6):723–751
29. Millán D, Rosolen A, Arroyo M (2013) Nonlinear manifold learning for meshfree finite deformation thin shell analysis. Int J Numer Methods Eng 93:685–713
30. Millán D, Arroyo M (2013) Nonlinear manifold learning for model reduction in finite elastodynamics. Comput Methods Appl Mech Eng 261262(0):118–131
31. Millán D, Arroyo M, Hashemian B (2013) B. Biasing molecular dynamics simulations with smooth and nonlinear data-driven collective variables. Submitted to Journal of Chemical Physics
32. Arroyo PAI, M Abdollahi A (2013) Effect of flexoelectricity on the electromechanical response of nano cantilever beams. Submitted to Journal of Computational Physics
33. Rosolen A, Peco C, Arroyo M (2013) An adaptive meshfree method for phase-field models of biomembranes Part I: approximation with maximum-entropy basis functions. J Comput Phys 249(0):303–319
34. Peco C, Rosolen A, Arroyo M (2013) An adaptive meshfree method for phase-field models of biomembranes Part II: a lagrangian approach for membranes in viscous fluids. Chin J Comput Phys 249(0):320–336
35. Rabczuk MD, Arroyo TM, Amiri F (2013) Phase-field modeling of fracture mechanics in linear thin shells. J Appl Math
36. Quaranta G, Kunnath SK, Sukumar N (2012) Maximum-entropy meshfree method for nonlinear static analysis of planar reinforced concrete structures. Eng Struct 42:179–189
37. Cyron CJ, Nissen K, Gravemeier V, Wall WA (2010) Stable meshfree methods in fluid mechanics based on greens functions. Comput Mech 46(2):287–300
38. Bonet J, Kulasegaram S (2000) Correction and stabilization of smooth particle hydrodynamics methods with applications in metal forming simulations. Int J Numer Methods Eng 47(6):1189–1214
39. Guo YM, Nakanishi K (2003) A backward extrusion analysis by the rigidplastic integrallessmeshless method. J Mater Process Technol 13(140):19–24. Proceedings of the 6th Asia Pacific Conference on materials Processing
40. Wen H, Dong X, Yan C, Ruan X (2007) Three dimension profile extrusion simulation using meshfree method. Int J Adv Manuf Tech 34(3-4):270–276
41. Wu CT, Chen JS, Pan C, Roque C (1998) A lagrangian reproducing kernel particle method for metal forming analysis. Comput Mech, 289
42. Chen JS, Roque CMOL, Chunhui P, Button ST (1998) Analysis of metal forming process based on meshless method. J Mater Process Technol, 642–646
43. Yoon S, Chen JS (2002) Accelerated meshfree method for metal forming simulation. Finite Elem Anal Des 38(10):937–948
44. Alfaro I, Yvonnet J, Cueto E, Chinesta F, Doblaré M (2006) Meshless methods with application to metal forming. Comput Methods Appl Mech Eng 195(489):6661–6675
45. Alfaro I, González D, Bel D, Cueto E, Doblar M, Chinesta F (2006) advances in the meshless simulation of aluminium extrusion and other related forming processes. Archives Comput Methods Eng 13(1):3–43
46. Alfaro I, Bel D, Cueto E, Doblaré M, Chinesta F (2006) Three-dimensional simulation of aluminium extrusion by the -shape based natural element method. Comput Methods Appl Mech Eng 195(33-36):4269–4286
47. Alfaro I, Gagliardi F, Olivera J, Cueto E, Filice L, Chinesta F (2009) Simulation of the extrusion of hollow profiles by natural element methods. Int J Mater Form 2(Supplement 1):597–600
48. Cueto E, Chinesta F (2013) Meshless methods for the simulation of material forming. Int J Mater Form, 1–19
49. Quak W, Gonzalez D, Cueto E, van den Boogaard AH (2009) On the use of local max-ent shape functions for the simulation of forming processes. In: Onate E, Owen DRJ (eds) X International Conference on Computational Plasticity, COMPLAS X. CIMNE, Barcelona, Spain
50. Chenot JL, Bellet M (1992) Numerical Modelling of Material Deformation Processes. In: Hartley P, Pillinger I, Sturgess C (eds). Springer, London, pp 179–224
51. Dolbow J, Belytschko T (1999) Volumetric locking in the element free Galerkin method. Int J Numer Methods Eng 46(6):925–942
52. González D, Cueto E, Doblaré M (2004) Volumetric locking in natural neighbour Galerkin methods. Int J Numer Methods Eng 61(4):611–632
53. Brezzi F (1974) On the existence, uniqueness and approximation of saddle-point problems arising from lagrangian multipliers. ESAIM: Math Model Numer Anal Modél Math Anal Numér 8(R2):129–151
54. Babuka I (1973) The finite element method with lagrangian multipliers. Numerische Mathematik 20(3):179–192
55. Li J, He Y, Chen Z (2009) Performance of several stabilized finite element methods for the stokes equations based on the lowest equal-order pairs. Computing 86(1):37–51
56. Ortiz A, Puso MA, Sukumar N (2010) Maximum-entropy meshfree method for compressible and near-incompressible elasticity. Comput Methods Appl Mech Eng 199(25–28):1859–1871
57. Arnold DN, Brezzi F, Fortin M (1984) A stable finite element for the stokes equations. CALCOLO 21(4):337–344
58. Ortiz A, Puso MA, Sukumar N (2011) Maximum-entropy meshfree method for incompressible media problems. Finite Elem Anal Des 47(6):572–585
59. Cyron CJ, Arroyo M, Ortiz M (2009) Smooth, second order, non-negative meshfree approximants selected by maximum entropy. Int J Numer Methods Eng 79(13):1605–1632
60. Rosolen A, Millán D, Arroyo M (2012) Second order convex maximum entropy approximants with applications to high order PDE. Int J Numer Methods Eng
61. González D, Cueto E, Doblaré M (2010) A higher-order method based on local maximum entropy approximation. Int J Numer Methods Eng 83(6):741–764
62. Bompadre A, Perotti LE, Cyron C, Ortiz M (2012) Convergent meshfree approximation schemes of arbitrary order and smoothness. Comput Methods Appl Mech Eng 221–222:83–103
63. Puso MA, Chen JS, Zywicz E, Elmer W (2008) Meshfree and finite element nodal integration methods. Int J Numer Methods Eng 74(3):416–446
64. Codina R (1998) Comparison of some finite element methods for solving the diffusion-convection-reaction equation. Comput Methods Appl Mech Eng 156(14s):185–210
65. Barth T, Bochev P, Gunzburger M, Shadid J (2004) A taxonomy of consistently stabilized finite element methods for the stokes problem. SIAM J Sci Comput 25(5):1585–1607
66. Bochev P, Gunzburger M (2004) An absolutely stable pressure-poisson stabilized finite element method for the stokes equations. SIAM J Numer Anal 42(3):1189–1207
67. Peco C, Rosolen A, Arroyo M (2013) Estabilización de las ecuaciones de stokes con aproximantes locales de máxima entropía. Submitted to RIMNI
68. Brezzi F, Pitkaranta J (1984) On the stabilization of finite element approximations of the Stokes equations. Notes on Numerical

Fluid Mechanics, Efficient Solutions of Elliptic Systems, vol 10. Viewig, Braunschweig, pp 11–19
69. Greco F, Sukumar N (2013) Derivatives of maximum-entropy basis functions on the boundary: theory and computations. Int J Numer Methods Eng 94(12):1123–1149
70. Hughes TJR, Franca LP, Balestra M (1986) A new finite element formulation for computational fluid dynamics: V. circumventing the babuka-brezzi condition: a stable Petrov-Galerkin formulation of the stokes problem accommodating equal-order interpolations. Comput Methods Appl Mech Eng 59(1): 85–99
71. Jansen KE, Collis SS, Whiting C, Shakib F (1999) A better consistency for low-order stabilized finite element methods. Comput Methods Appl Mech Eng 174(1-2):153–170
72. Harari I, Hughes TJR (1992) What are C and h?: Inequalities for the analysis and design of finite element methods. Comput Methods Appl Mech Eng 97(2):157–192
73. Wriggers P (2003) Computational contact mechanics. Comput Mech 32:141–141
74. Hormann K, Sukumar N (2008) Maximum entropy coordinates for arbitrary polytopes. In: Proceedings of SGP 2008
75. Edelsbrunner H, Kirkpatrick D, Seidel R (1983) On the shape of a set of points in the plane. IEEE Trans Inform Theory 29(4):551–559
76. Kalpakjian S (1992) Manufacturing Processes for Engineering Materials, 5/e (New Edition). Pearson Education
77. Quak W., Boogaard A. H., Hutink J (2009) Meshless methods and forming processes. Int J Mater Form 2(1):585–588
78. Ceretti E, Taupin E, Altan T (1997) Simulation of metal flow and fracture applications in orthogonal cutting, blanking, and cold extrusion. CIRP Ann-Manuf Technol 46(1):187–190
79. Arrazola PJ, zel T, Umbrello D, Davies M, Jawahir IS (2013) Recent advances in modelling of metal machining processes. CIRP Ann-Manuf Technol 62(2):695–718